ARMY RESEARCH LABORATORY

Temperature Dependence of a Diode-pumped Cryogenic Erbium (Er):Yttrium Aluminum Garnet (YAG) Laser

by Larry D. Merkle, Nikolay Ter-Gabrielyan, G. Alex Newburgh, Arockiasamy Michael, and Mark Dubinskii

ARL-TR-4885 **July 2009**

NOTICES

Disclaimers

The findings in this report are not to be construed as an official Department of the Army position unless so designated by other authorized documents.

Citation of manufacturer's or trade names does not constitute an official endorsement or approval of the use thereof.

Destroy this report when it is no longer needed. Do not return it to the originator.

Army Research Laboratory
Adelphi, MD 20783-1197

ARL-TR-4885 **July 2009**

Temperature Dependence of a Diode-pumped Cryogenic Erbium (Er):Yttrium Aluminum Garnet (YAG) Laser

Larry D. Merkle, Nikolay Ter-Gabrielyan, G. Alex Newburgh, Arockiasamy Michael, and Mark Dubinskii
Sensors and Electron Devices Directorate, ARL

REPORT DOCUMENTATION PAGE	Form Approved OMB No. 0704-0188

1. REPORT DATE *(DD-MM-YYYY)*	2. REPORT TYPE	3. DATES COVERED (From - To)
July 2009	Summary	

4. TITLE AND SUBTITLE
Temperature Dependence of a Diode-pumped Cryogenic Erbium (Er):Yttrium Aluminum Garnet (YAG) Laser

5a. CONTRACT NUMBER

5b. GRANT NUMBER

5c. PROGRAM ELEMENT NUMBER

6. AUTHOR(S)
Larry D. Merkle, Nikolay Ter-Gabrielyan, G. Alex Newburgh, Arockiasamy Michael, and Mark Dubinskii

5d. PROJECT NUMBER

5e. TASK NUMBER

5f. WORK UNIT NUMBER

7. PERFORMING ORGANIZATION NAME(S) AND ADDRESS(ES)
U.S. Army Research Laboratory
Attn: RDRL-SEE-O
2800 Powder Mill Road
Adelphi, MD 20783-1197

8. PERFORMING ORGANIZATION REPORT NUMBER
ARL-TR-4885

9. SPONSORING/MONITORING AGENCY NAME(S) AND ADDRESS(ES)

10. SPONSOR/MONITOR'S ACRONYM(S)

11. SPONSOR/MONITOR'S REPORT NUMBER(S)

12. DISTRIBUTION/AVAILABILITY STATEMENT
Approve for public release; distribution unlimited.

13. SUPPLEMENTARY NOTES

14. ABSTRACT
We report the laser performance of resonantly diode-pumped erbium (Er):yttrium aluminum garnet (YAG) from liquid nitrogen temperature to above room temperature. Relative to incident pump power, the best performance was observed at approximately 160 K. Spectroscopy and modeling show that this is due primarily to the changing efficiency of diode pump absorption as the absorption lines broaden with temperature. However, the physics of the Er:YAG system indicates that even with an arbitrarily narrow pump linewidth the most efficient laser performance should occur at a temperature somewhat above 77 K. The causes of the temperature dependence are at least qualitatively understood.

15. SUBJECT TERMS
Solid state laser, diode pumped, Er:YAG, thermal effects

16. SECURITY CLASSIFICATION OF:			17. LIMITATION OF ABSTRACT	18. NUMBER OF PAGES	19a. NAME OF RESPONSIBLE PERSON
a. REPORT	b. ABSTRACT	c. THIS PAGE			Larry D. Merkle
Unclassified	Unclassified	Unclassified	UU	32	19b. TELEPHONE NUMBER (*Include area code*) (301) 394-0941

Standard Form 298 (Rev. 8/98)
Prescribed by ANSI Std. Z39.18

Contents

List of Figures

List of Tables

Acknowledgment

We gratefully acknowledge financial support for this work from the High Energy Laser Joint Technology Office.

Summary

We report the laser performance of resonantly diode-pumped erbium (Er):yttrium aluminum garnet (YAG) from liquid nitrogen temperature to above room temperature. Relative to incident pump power, the best performance was observed at approximately 160 K. Spectroscopy and modeling show that this is due primarily to the changing efficiency of diode pump absorption as the absorption lines broaden with temperature. However, the physics of the Er:YAG system indicates that even with an arbitrarily narrow pump linewidth the most efficient laser performance should occur at a temperature somewhat above 77 K. The temperature dependence of the laser wavelength is satisfactorily explained by comparing the stimulated emission cross section of each candidate laser line with the losses due to ground-state absorption (GSA) and output coupling. The decrease in laser performance above 160 K, however, is only qualitatively understood. A good fit to the output energy data can be obtained assuming the correct shape for the temperature dependence of laser threshold but requires multiplying that threshold by a factor of several.

INTENTIONALLY LEFT BLANK.

1. Introduction

For solid-state lasers, and particularly for their high power operation, it is very desirable to keep the quantum defect as low as possible, so that heat deposition in the gain medium is minimized. Although cross-relaxation can reduce thermal loading by other means in some systems (*1, 2*), quantum defect reduction usually requires pumping the laser ion into the same excited state manifold as the upper laser level. This pumping approach, often called "resonant pumping," has become feasible in recent years, largely due to diode pumping and the development of diode lasers at an increasing range of wavelengths. Such small-quantum-defect pumping has been pursued to good effect for the ytterbium (Yb^{3+}) laser ion for several years (*3, 4*), and more recently it has been possible to apply the same ideas to the erbium (Er^{3+}) ion, in some cases pumped by an Er-doped fiber laser (*5–7*), and still more recently pumped by diode lasers (*6, 8, 9*). Er^{3+} is an attractive laser ion, since its laser wavelengths are in spectral regions where the eye is far less susceptible to laser-induced damage than is true of Yb^{3+} (*10*).

Where thermal management is important, crystalline hosts for the laser ion are preferred over glass due to their generally superior thermal conductivity. Yttrium aluminum garnet (YAG) is a particularly interesting crystalline host. Its success in many laser applications over nearly the full history of the laser is due to its attractive combination of spectroscopic and thermomechanical properties, and the resulting extensive development of YAG crystal growth makes it a relatively mature laser host. Thus, it is not surprising that much of the work on resonantly pumped Er lasers has focused on Er:YAG (*5–9*), and this material continues to be of great interest.

In recent years, there has been increasing interest in cryogenic solid-state lasers. Of course, early lasers were often operated at cryogenic temperatures to counteract the deleterious effects of thermal quenching and ground-state absorption (GSA) in systems with relatively low crystal quality and inefficient pumping mechanisms (*11*). By contrast, the recent resurgence of interest in cryogenic solid-state lasers has been driven by the same concerns for thermal management that drive much of the interest in resonant pumping. Crystalline materials have higher thermal conductivity at low temperatures than at room temperature, and many materials also exhibit smaller values of the thermal expansion and thermo-optic coefficients (*12–14*). Impressive results have been obtained, particularly for cryogenic Yb lasers (*15, 16*).

We have recently undertaken investigations of cryogenic operation of Er lasers, including Er:YAG (*17–19*). In this report, we report in more detail the results of our study of Er:YAG laser operation from liquid nitrogen temperature to above room temperature. This includes presentation and interpretation of the temperature dependence of the laser output power and wavelength in terms of the spectroscopy of Er^{3+} in YAG.

2. Experimental Details

The Er:YAG samples investigated in this study are from two sources. Ceramic YAG with 0.5 atomic % Er was obtained from the Konoshima Chemical Company. A sample of this material 0.283 cm thick was used for absorption spectra, and another piece of this material was powdered to minimize reabsorption for fluorescence spectra and lifetime data. A 2 atomic % Er:YAG single-crystal sample from Scientific Materials was fabricated to be 1.0 cm long with both lateral dimensions 0.5 cm, and the 0.5×0.5 cm^2 ends were antireflection coated for both the pump and laser wavelength ranges. Due to the nearly equal ionic radii of Y^{3+} and Er^{3+}, we take the segregation coefficient of Er in YAG to be sufficiently close to 1.0 that we use these nominal concentrations as correct (*20*). We treat spectra taken on the 0.5% Er:YAG ceramic material as valid for single-crystal Er:YAG, based on the nearly identical spectroscopy of Er reported for ceramic and single-crystalline YAG (*21, 22*).

Spectroscopic data were taken using several apparatus. Absorption spectra were taken on a Varian Cary 6000i spectrophotometer, with care taken to narrow the slits to get sufficient resolution at the lowest temperatures. Emission spectra were taken on an Acton SpectraPro 2500i 0.5-m monochromator equipped with a Sciencetech thermoelectrically cooled indium gallium arsenide (InGaAs) detector. Excitation for these emission spectra was accomplished by using a temperature stabilized 975-nm fiber coupled laser diode.

For fluorescence decay (lifetime) data, the excitation source was a 975-nm fiber coupled laser diode in pulsed mode (~1–1.5 ms). The decay waveforms were captured using a Tektronix TDS 7104 digitizing oscilloscope.

For spectroscopic measurements, the temperature was controlled using a Janis CCS-350 cryogenic refrigerator.

3. Laser Data

Laser experiments were performed using the apparatus diagrammed in figure 1. The Er:YAG laser crystal was mounted on a copper cold plate inside a boil-off liquid nitrogen cryostat. It was quasi-continuous wave (CW) pumped with a 10-bar microchannel-cooled laser diode array (Princeton Lightwave) with corrected fast and slow axis divergences. This indium gallium arsenide phosphide (InGaAsP)/indium phosphide (InP) diode bar stack was designed specifically for resonant pumping of Er^{3+}. It had a spectral full width at half maximum of approximately 9 nm, was centered at 1530 nm, and had its temperature tuned to achieve maximum laser output. The pump was delivered through a dichroic mirror (which also served as the high reflector of the

laser cavity) with a combination of cylindrical lenses yielding an oblong 80×400 micrometer focal spot. The Rayleigh range of the pump beam was observed to be approximately 0.25 cm in air, significantly shorter than the laser crystal, so that the average pump beam area was considerably larger than its value at focus. The cavity length was 10 cm, defined by the high reflector and by an output coupler with a 25-cm radius of curvature. Due to the cavity mirrors being outside the liquid nitrogen cryostat, the sample sat at approximately the center of the cavity, where the lowest-order mode would have a radius at e^{-2} intensity of about 250 μm. We have observed the output beam to have a shape similar to the pump beam, and thus to be multimode.

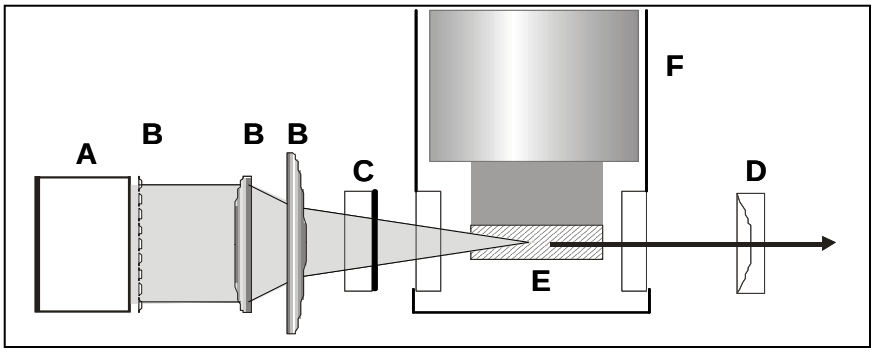

Figure 1. Apparatus for low-temperature laser experiments—A: pump laser diode array, B: pump beam focusing optics, C: dichroic mirror, D: output coupler, E: Er:YAG laser gain medium, and F: liquid nitrogen optical cryostat.

The pump pulses were 5 ms in duration, and the pulse repetition frequency was set to 2 Hz. As will be discussed later, only a modest fraction of the pump light was absorbed, and for this reason the data are presented in terms of absorbed pump power. The fraction absorbed can be increased by optimizing the sample length and by double-passing the pump.

The typical quasi-CW performance of a 2% Er:YAG laser operated at about liquid nitrogen temperature is shown in figure 2. The performance of this laser was rather satisfactory, in view of the non-ideal pump beam shape. With an approximately optimal output coupler reflectivity of 90%, the laser threshold was 66 mJ absorbed and the optical-to-optical slope efficiency was 0.66, referred to absorbed pump energy.

We have investigated the temperature dependence of this laser by fixing the incident pump energy at 2.1 J per pulse and monitoring the laser output as the temperature was varied. The results are shown in figure 3. There was a striking increase in output from liquid nitrogen temperature up to about 160 K, followed by a decrease as the temperature was further increased to room temperature and beyond. The reasons for this behavior will be discussed in section 5. We observed that the laser wavelength was 1618 nm below about 90 K, 1645 nm above 110 K, and that both lines could be observed between those temperatures. This behavior, too, will be discussed in section 5. Before these discussions can be given, we must note some details of the spectroscopy of Er:YAG.

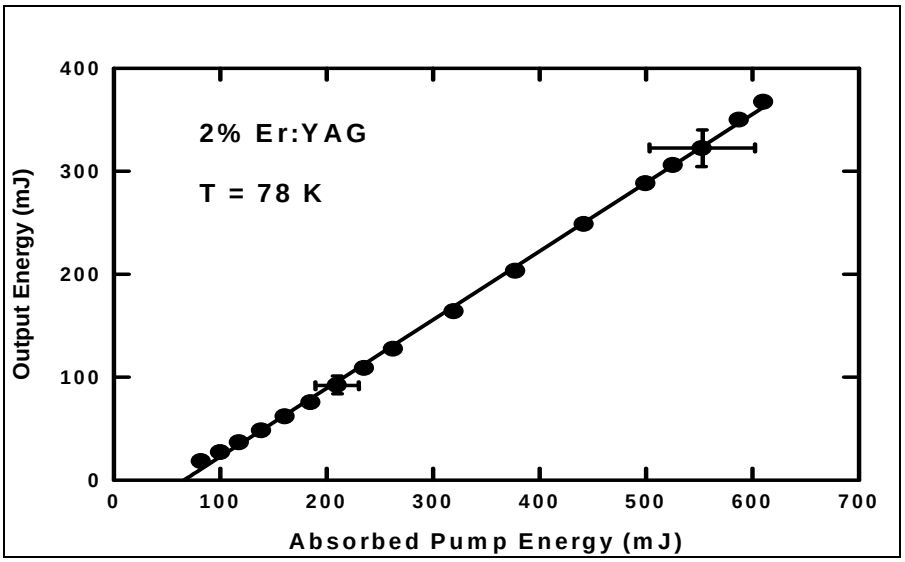

Figure 2. Laser performance of 2% Er:YAG at approximately 78 K, with output coupler reflectivity = 0.9. The error bars represent the estimated uncertainty of ±10% for the absorbed pump and ±5% for the output.

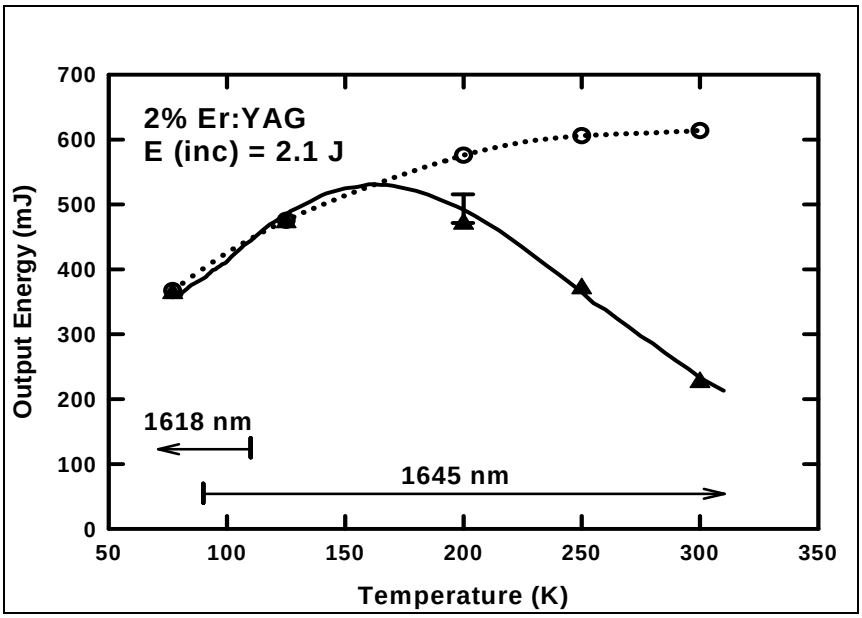

Figure 3. Laser output of 2% Er:YAG vs. temperature for fixed incident pump power—solid curve: experimental data; open circles: fit with pump area = 0.050 cm^2 and mode fill efficiency = 0.5; dotted curve: a guide to the eye; and filled triangles: fit with pump area = 0.35 cm^2 and mode fill efficiency = 0.6. The error bar represents the ±5% uncertainty in output energy.

4. Spectroscopic Data

The spectroscopy of Er^{3+} in both single-crystal and ceramic YAG has been studied rather extensively, at both room temperature (*22–24*) and cryogenic temperatures (*21, 23, 25–27*). Thus, we concentrate our discussion on the temperature dependence of the absorption and stimulated emission cross section spectra in the region covering the observed laser lines, and the absorption spectra in the pump wavelength region.

The absorption spectrum of Er:YAG due to transitions from the ground manifold, $^4I_{15/2}$, to the first excited manifold, $^4I_{13/2}$, is given as a function of temperature in figure 4. At the lowest temperature there are relatively few absorption lines, as only the lowest state in the $^4I_{15/2}$ manifold is occupied to a significant degree. As the temperature increases, additional lines grow in due to thermal occupation of higher levels, and these additional lines prove important for both pumping and laser emission in this material. The other familiar effect of increased temperature, the broadening of narrow absorption lines, is seen more clearly in figure 5. There is also evidence in these spectra that the line at approximately 1532 nm grows as the temperature is increased from 8 K to 150 K, indicating that this transition initiates on a state above the ground state. The strength of this line is very interesting for diode pumped laser operation, as the use of the longest-wavelength pump line with sufficient strength enables minimization of the quantum defect between the pump and laser transitions, thus minimizing thermal distortions. A still closer inspection of this spectral region is given in figure 6, showing that, although the ~1532-nm peak's height is maximum at about 150 K, the decrease in height up further temperature increase is due to thermal broadening, so that the wavelength-integrated strength of this peak stays about constant at higher temperatures. It is also clear that several smaller absorption lines grow in as the temperature is increased, similar to the temperature dependence of the ~1532-nm line. These lines are weaker, but since the pump diode array available for the current study has a linewidth of about 9 nm, their presence contributes to pump absorption.

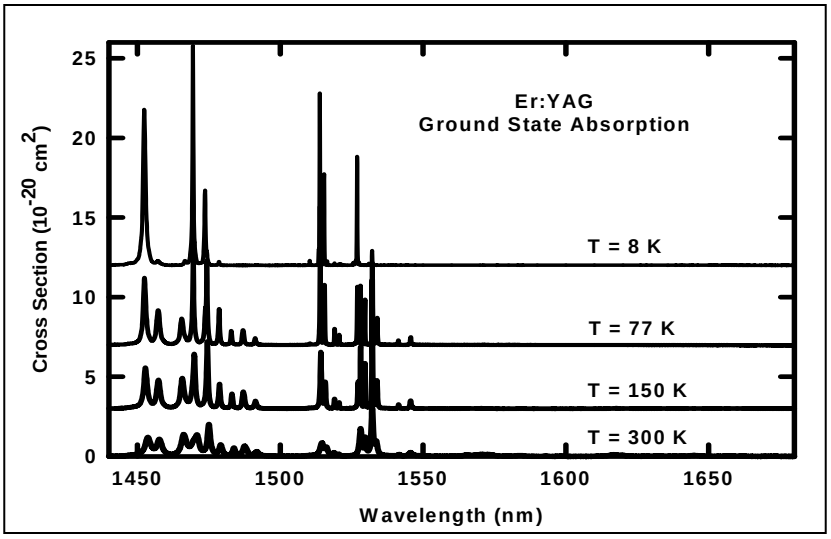

Figure 4. GSA cross-section of Er:YAG at four temperatures. The baselines are offset for clarity.

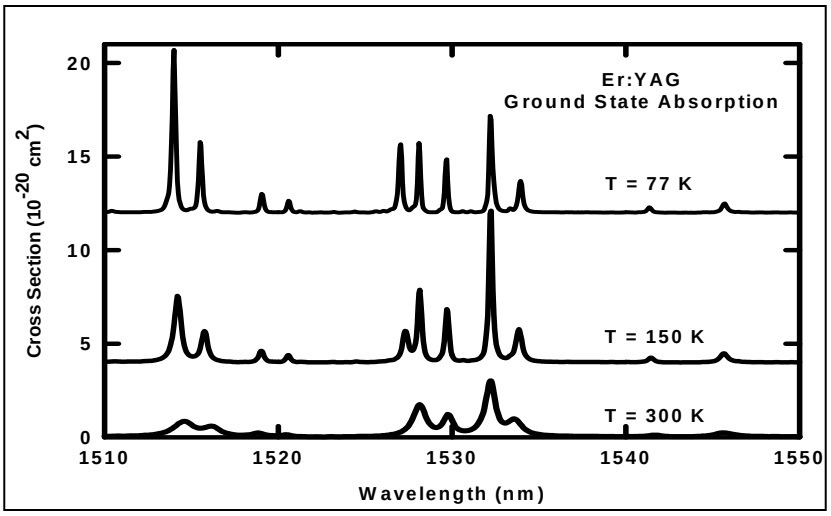

Figure 5. GSA cross-section spectra of Er:YAG—detail of the region with the sharpest lines.

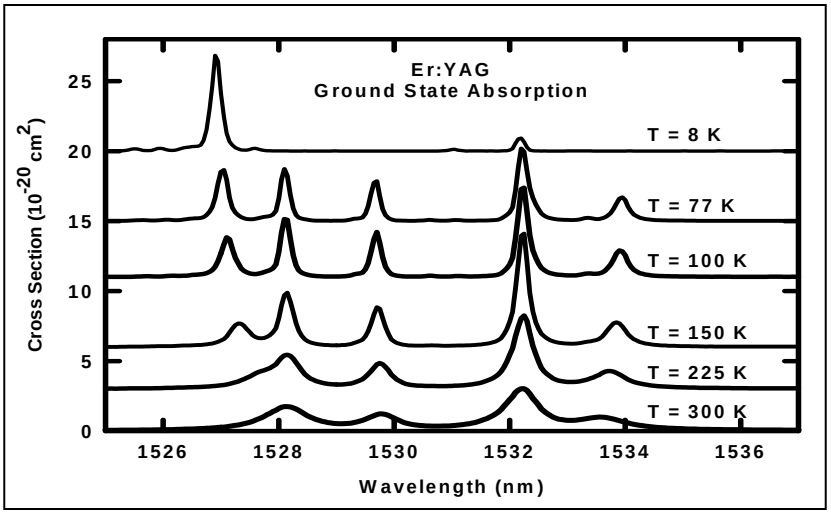

Figure 6. GSA cross section spectra of Er:YAG vs. temperature—detail of diode-pumping region.

In addition, the shifting of some lines in figure 6 shows that some energy levels of Er^{3+} in YAG change with temperature. A much more complete set of spectral data would be required to analyze these changes in terms of the temperature dependence of the Er ion's environment, a task that is beyond the scope of this study.

It is also important to consider how the stimulated emission cross-section spectrum changes with temperature. We have calculated this spectrum for transitions from the $^4I_{13/2}$ to the $^4I_{15/2}$ manifold by two methods. The reciprocity method calculates the stimulated emission cross sections for a given temperature from absorption cross sections and knowledge of the energy level positions and degeneracies (*24*). The Fuchtbauer-Ladenburg (F-L) method obtains stimulated emission from the fluorescence spectrum and the known (or estimated) radiative decay rate (*28*). The two methods have complementary strengths and weaknesses. Reciprocity is effective only on transitions for which the lower level has sufficient thermal population to give adequate absorption, and thus at cryogenic temperatures the emission transitions ending on high-lying members of the ground manifold cannot be determined by this method. Since these are the very transitions with the greatest likelihood of providing net gain, this limitation is significant. The F-L method avoids this problem by using the measured fluorescence spectrum, but it relies on knowing the radiative lifetime of the upper manifold, which is not always equal to the observed fluorescence lifetime due to quenching and reabsorption. Also, for emission lines at wavelengths where the absorption is strong, reabsorption may significantly reduce the apparent emission strength, even when care is taken to use thin layers of powder to minimize that problem.

We obtained the required spectra at several temperatures using equipment described in section 2, and inferred the radiative decay rate from fluorescence lifetime data discussed later in this section. The results are shown for the full $^4I_{13/2} \rightarrow {}^4I_{15/2}$ spectra at liquid nitrogen and room

temperatures in figure 7. The limitation of reciprocity noted previously is responsible for the lack of data from that method at 77 K. Also, note that at both temperatures the narrow, strong lines between 1510 and 1540 nm are weaker in the F-L spectra than in the reciprocity spectra. Since these lines have practically identical widths in both absorption and fluorescence, this difference cannot be attributed to instrumental broadening. Instead, it almost certainly indicates the effect of reabsorption on the observed fluorescence line strength, exemplifying one of the limitations noted for the F-L method. However, the lines at wavelengths longer than 1550 nm at 300 K, where they are available from both methods, are very nearly the same strength. This gives confidence that the stimulated emission cross sections obtained by F-L are reasonably accurate for wavelengths in this range. This is important, since this is the spectral range in which net gain is most readily achieved, as noted previously.

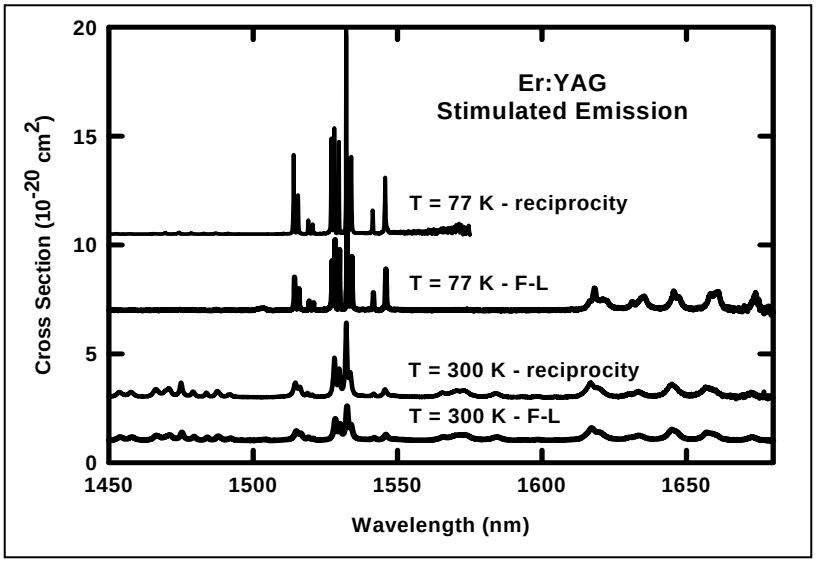

Figure 7. Comparison of $^4I_{13/2} \rightarrow {}^4I_{15/2}$ stimulated emission spectra of 0.5% Er:YAG calculated by two methods.

The stimulated emission and absorption spectra of 0.5% Er:YAG over the emission wavelength range relevant to this study are compared for three representative temperatures in figure 8. At sufficiently low temperatures laser action was observed at 1618 nm, as would be anticipated based on the 77-K spectra. This peak is somewhat stronger than the 1645-nm peak, and at this low temperature neither line contends with significant GSA. However, by 150 K GSA at the 1618-nm peak is already perceptible, and is (of course) larger than that at the 1645-nm peak. Since the difference in GSA is small, it is not obvious by eye that this difference will force laser operation to prefer the 1645-nm line. Modeling results, to be presented in section 5, are required to see that the small GSA at 1618 nm is indeed enough to switch the laser wavelength. By 300 K, it is clear that the stimulated emission cross sections are reduced due to line broadening and that the GSA cross sections are substantially higher. Thus, it is to be expected that the laser threshold will be higher at room temperature than at lower temperatures.

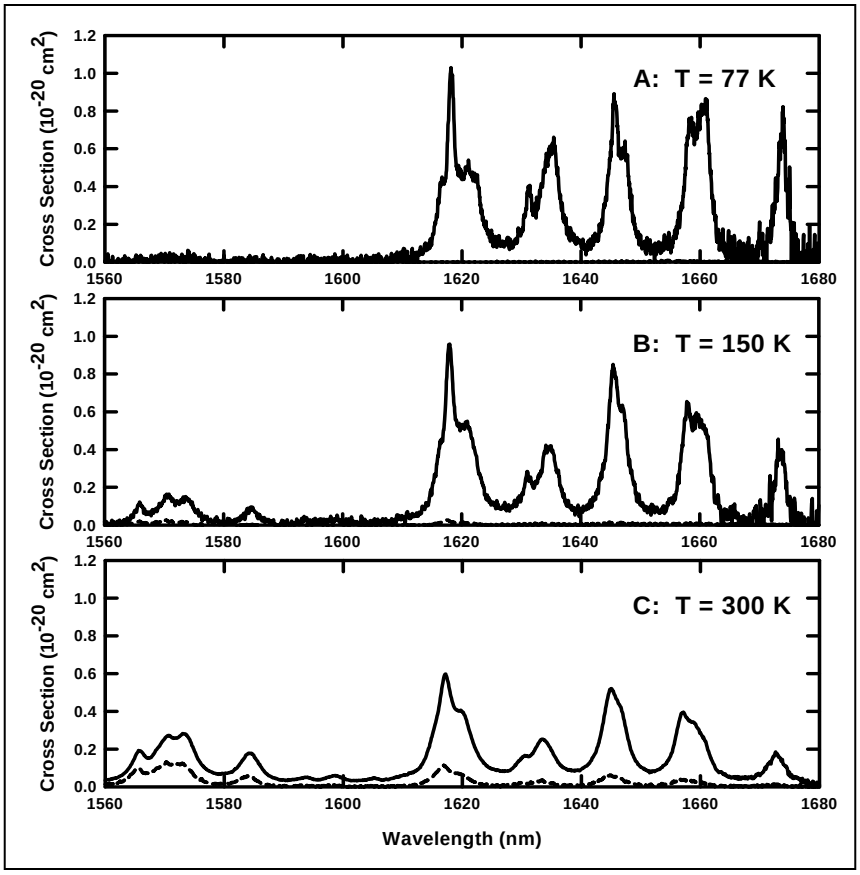

Figure 8. GSA (dashed curves) and stimulated emission (solid curves) spectra of 0.5% Er:YAG at 77, 150, and 300 K.

To convert the fluorescence spectra into stimulated emission data, the radiative lifetime is needed. We observed the fluorescence decay kinetics of 0.5% Er:YAG at both 1618 and 1645 nm, following excitation by 1.5-ms pulses at 975 nm, which pumps the Er^{3+} $^4I_{11/2}$ manifold. Decay from that manifold to the $^4I_{13/2}$ metastable state is sufficiently fast not to obscure the $^4I_{13/2}$ relaxation relevant to this study. Example waveforms are given in figure 9 for emission at 1618 nm at two temperatures. Note that the decays are almost purely exponential, after a rise time that is largely due to the pump pulse duration but that is probably lengthened somewhat by the $^4I_{11/2}$ decay time. The inset shows that there is a very small contribution due to a faster decay that is just discernable over the first several milliseconds. This may indicate the presence of weak quenching or upconversion, but it does not interfere with extraction of a fluorescence lifetime value from the later portion of the decay. Indeed, these faster processes are so weak that no attempt was made to analyze them. Not surprisingly, the exponential decay rates for the two emission lines are practically identical. The results are summarized in table 1. We believe these lifetimes to be good approximations to the radiative lifetimes, for a combination of reasons: the exponential decay waveforms, our use of powder to minimize radiative reabsorption, and the low Er concentration, which reduces the probability of upconversion and other ion-ion quenching

processes. Note that there are thermally activated emission bands of significant size compared to the low-temperature emission bands, as exemplified in the 1560–1600-nm region of figure 8. The transitions in that spectral range appear to be strong enough that their growth with increasing temperature increases the total emission rate. Thus, the reduction in lifetime with increasing temperature is consistent with the assumption of radiative decay. These fluorescence lifetimes were used in the F-L calculations that yield the stimulated emission spectra of figure 8.

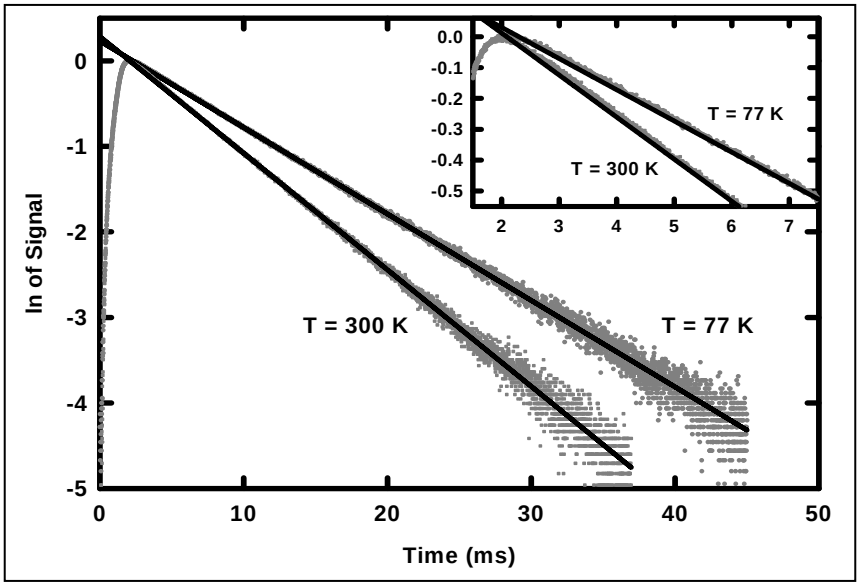

Figure 9. Fluorescence decay waveforms of 0.5% Er:YAG powder at 1618 nm for two temperatures. Gray symbols: experimental data; black lines: single exponential fits; and inset: the initial portions of the same waveforms.

Table 1. Temperature (T) dependence of the fluorescence lifetime of 0.5% Er:YAG, averaged over the two emission wavelengths.

T (K)	**Lifetime, each ± 0.04 (ms)**
77	9.86
150	8.54
225	7.80
300	7.34

The temperature dependence of the absorption spectra can also affect the efficiency with which pump light is absorbed. To obtain a useful approximation to this absorption efficiency, we have used the emission spectrum of the laser diode pump array and the absorption spectra in the same wavelength range to calculate the fraction of pump light absorbed for several temperatures. The calculated transmitted diode pump spectra are given for 77 and 300 K in figure 10, along with the incident pump spectrum, for the 1.0-cm thick laser sample with 2% Er concentration. Clearly, these calculations indicate that much more of the pump light is absorbed at room

temperature than at liquid nitrogen temperature. At the wavelengths of some peaks, there is actually less absorption at room temperature due to the reduced peak cross sections, but temperature broadening of the absorption lines more than compensates for this. The resulting fraction of pump light absorbed is given for several temperatures in table 2. Interpolated values are given for temperatures at which emission data were taken. These calculations are approximations, in that they assume the absorption spectra observed at low light levels apply to all pumping levels. In laser operation, some bleaching must take place to overcome the non-zero absorption at the laser wavelengths. However, this absorption is small compared to the stimulated emission, so that the amount of bleaching required is also small and thus the approximation involved in figure 10 and table 2 is a reasonable one.

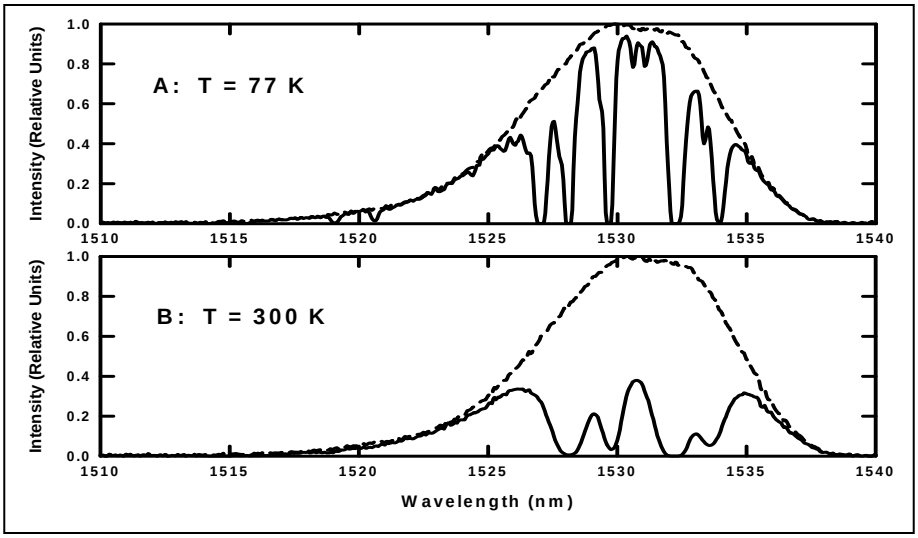

Figure 10. Single-pass transmission of the diode laser array pump by 2% Er:YAG laser sample at two temperatures. Dashed curve: incident pump spectrum and solid curve: calculated transmitted pump spectrum.

Table 2. Temperature (T) dependence of the fraction of diode pump power absorbed, based on spectroscopically determined absorption.

T (K)	Fraction Absorbed, F_{pump} Experimental	Fraction Absorbed, F_{pump} Interpolated
77	0.38	
100	0.43	
125		0.50
150	0.55	
200		0.62
225	0.65	
250		0.67
300	0.70	

5. Interpretation

The principal features of the laser data to be explained are the temperature dependence of the laser output for constant incident pump power and the change in laser wavelength with temperature. The spectroscopic features noted previously suggest the likely causes for these behaviors. The switch in laser wavelength is expected to be due to the growth in GSA with temperature. The rise in laser output with temperature up to about 160 K can be attributed, at least primarily, to the increased efficiency of pump absorption with temperature; whereas, the fall in output for higher temperatures is expected to be attributable to the increase in GSA and decrease in stimulated emission cross sections at the laser wavelength. In this section, we will apply simple models to see if these expectations are borne out by our data.

To determine which emission line should lase at a given temperature, we can apply the familiar threshold condition as follows:

$$g_{net} = \sigma_{true} \cdot n_{Er} \cdot 2L_{gain} \cdot \left(f_{exc} \cdot f_{UL} - \left(1 - f_{exc}\right) \cdot f_{LL} \right) + \ln\left(R_{OC}\right) \geq 0 \qquad (1)$$

Here, g_{net} is the net gain parameter for the laser cavity, and σ_{true} is the true cross section of the transition between the upper and lower laser levels, obtained from the observed GSA or stimulated emission cross section by correcting for the fractional thermal occupation of the initial state. n_{Er} is the Er^{3+} concentration and L_{gain} is the length of the gain medium (the laser crystal). f_{exc} is the fraction of Er ions excited, and f_{UL} and f_{LL} are the fractional thermal populations of the upper and lower laser levels, respectively, which become simply the ratio of the Boltzmann factors to the corresponding partition functions since the degeneracy factors for all levels equal two for Er in YAG. R_{OC} is the reflectance of the output coupler and $(1 - R_{OC})$ is taken to approximate the total passive loss. The Boltzmann factors and partition functions require the energy level spacings, obtained from Kaminskii as corrected by Setzler et al. (*6, 29*).

Sufficient cross-section data were taken at five temperatures, and the relevant parameters for those temperatures are given in table 3. The temperature-independent parameters are $n_{Er} = 2.78 \times 10^{20}$ cm^{-3} and $R_{OC} = 0.9$. For each temperature and each transition (1618 and 1645 nm), g_{net} was calculated for a range of f_{exc} values using equation 1. For all temperatures g_{net} was larger at 1645 nm than at 1618 nm for very small fractions excited, due to the larger GSA at 1618 nm, but the gain grew faster for 1618 nm due to that line's larger stimulated emission cross section. For 77 K, the calculation gives a positive g_{net} for the 1618-nm line at a lower excited fraction than for the 1645-nm line. For temperatures of 125 K and higher, g_{net} becomes positive first for the 1645-nm line, due to the increased GSA at 1618 nm. These results are consistent with the observed behavior, which gives 1618-nm laser operation below 90 K, 1645-nm operation above 110 K, and both wavelengths for temperatures between 90 and 110 K.

Thus, although one would not expect such a simple model (with no passive loss other than the output coupling and with the spatial variation of the excited fraction neglected) to work perfectly, it appears that the basic physics of the wavelength change with temperature is understood.

Table 3. Temperature (T)-dependent parameters used in laser wavelength and power models. The meanings of the symbols are given in the text.

T (K)	f_{UL} (1618 nm)	f_{LL} (1618 nm)	f_{UL} (1645 nm)	f_{LL} (1645 nm)	σ_{true} (1618 nm) (cm^2)	σ_{true} (1645 nm) (cm^2)
77	0.19	1.9×10^{-4}	0.19	2.5×10^{-5}	4.1×10^{-20}	3.5×10^{-20}
125	0.23	0.0031	0.23	8.8×10^{-4}	3.7×10^{-20}	3.3×10^{-20}
200	0.23	0.016	0.23	0.0071	3.1×10^{-20}	2.9×10^{-20}
250	0.22	0.026	0.22	0.014	3.0×10^{-20}	2.8×10^{-20}
300	0.21	0.036	0.21	0.022	2.9×10^{-20}	2.7×10^{-20}

To determine whether the temperature dependence of the output power is also adequately understood, a model is needed that can predict laser threshold and slope efficiency, and thus output power for a given pump power. We have chosen to apply the quasi-three level CW laser model of Beach (*30*). Although this model was developed for Yb^{3+} lasers, it is readily adaptable to Er^{3+} by substitution of the appropriate energy levels, with one proviso. Due to the sparse energy level structure of Yb^{3+}, upconversion is not a significant issue for that ion and is not taken into account in the Beach model. Since upconversion is an issue for Er^{3+}, the model will work well only for sufficiently low concentrations.

Since our diode laser array pump is sufficiently broad-band to pump several transitions at once, we have modified the Beach model. We have replaced its explicit dependence on the cross section and upper and lower level populations of a presumed single pump transition with the fraction of pump light absorbed, resulting in the following expressions:

$$\eta_{slope} = F_{pump} \cdot \eta_M \cdot \frac{\nu_L}{\nu_P} \cdot \frac{1 - R_{OC}}{R_{OC}} \cdot \frac{1}{\left(\exp(\sigma_{true} \cdot N_{21}) - 1\right) \cdot (T^2 \cdot \exp(\sigma_{true} \cdot N_{21}) + 1)} \tag{2}$$

$$P_{thr} = \frac{h \nu_P \cdot N_2 \cdot A}{F_{pump} \cdot \tau} \tag{3}$$

Here η_{slope} is the slope efficiency with respect to incident pump power; F_{pump} is the fraction of pump power absorbed; η_M is the efficiency of laser mode filling of the pumped volume; ν_L and ν_p are the laser and pump photon frequencies; σ_{true} is the true cross section at the laser wavelength; T is the single-pass transmittance of the cavity, taking into account only passive losses other than output coupling; h is Planck's constant; A is the cross-sectional area of the

pumped region; and τ is the upper laser level storage time (lifetime.) N_2 and N_{2l} are given as follows:

$$N_2 = \frac{f_{LL} \cdot n_{Er} \cdot L_{gain} + \frac{\ln\left(\frac{1}{T^2 \cdot R_{OC}}\right)}{2\sigma_{true}}}{f_{LL} + f_{UL}} \tag{4}$$

$$N_{21} = \left(f_{LL} + f_{UL}\right) \cdot N_2 - f_{LL} \cdot n_{Er} \cdot L_{gain} \tag{5}$$

As noted in section 3, the pump beam at focus has a cross-sectional area of roughly 0.025 cm^2, but averaged over the length of the gain medium A must be somewhat larger. The observed output beam is not clean enough to facilitate calculation of its cross-sectional area in the cavity, so that η_M is best treated as an adjustable parameter. Model calculations were performed using ROC = 0.9 (as used in the experiments), F_{pump} from table 2, τ from table 1, and the parameters from table 3. Assuming as before that the output coupling is the only passive loss, thus T = 1, we find that with A = 0.050 cm^2 (a plausible value for the average pump area) and η_M = 0.5 the increase in output power at low temperatures for a pump power of 420 W (2.1 J in a pulse of 5°ms) can be fit rather well. However, with these parameters the laser threshold does not rise sufficiently to reproduce the fall-off of output at higher temperatures, as shown by the open circles in figure 3. To achieve a good fit to the overall temperature dependence of the output power (and thus pulse energy) we must adjust the mode fill efficiency slightly, to 0.6, but must assume a far larger pump area of 0.35 cm^2. The resulting temperature dependence is shown by the solid triangles in figure 3.

The model calculations and equation 2 indicate that the slope efficiency, if calculated relative to absorbed (rather than incident) pump power or energy, is essentially independent of temperature except at the transition between 1618-nm and 1645-nm lasing. By contrast, the threshold absorbed pump pulse energy varies substantially with temperature, as shown in figure 11. On that figure, we also plot the absorbed pump pulse energy as function of temperature for fixed incident pump energy, consistent with table 2. These calculations and equation 3 make it clear how the artificially large pump area forces laser output for fixed incident pump to decrease at sufficiently high temperatures. It simply scales up the laser threshold so that the difference between absorbed pump energy and threshold energy decreases at high temperatures.

6. Discussion and Conclusions

The calculations given in section 5 indicate that the rise in output power from 77 to about 160 K is due primarily to the increased pump efficiency attributable to the large pump bandwidth. With a pump source narrower than the pumped absorption line, the increase in pump efficiency with temperature would be greatly reduced. However, some rise in laser output with temperature can be expected even with an arbitrarily narrow pump line. The upper laser level for both the 1618-nm and 1645-nm lines is approximately 58 cm^{-1} above the bottom of the $^4I_{13/2}$ manifold, so that thermal activation increases the population of this level rapidly up to liquid nitrogen temperature, and the increase remains significant even to somewhat higher temperatures (*6, 29*).

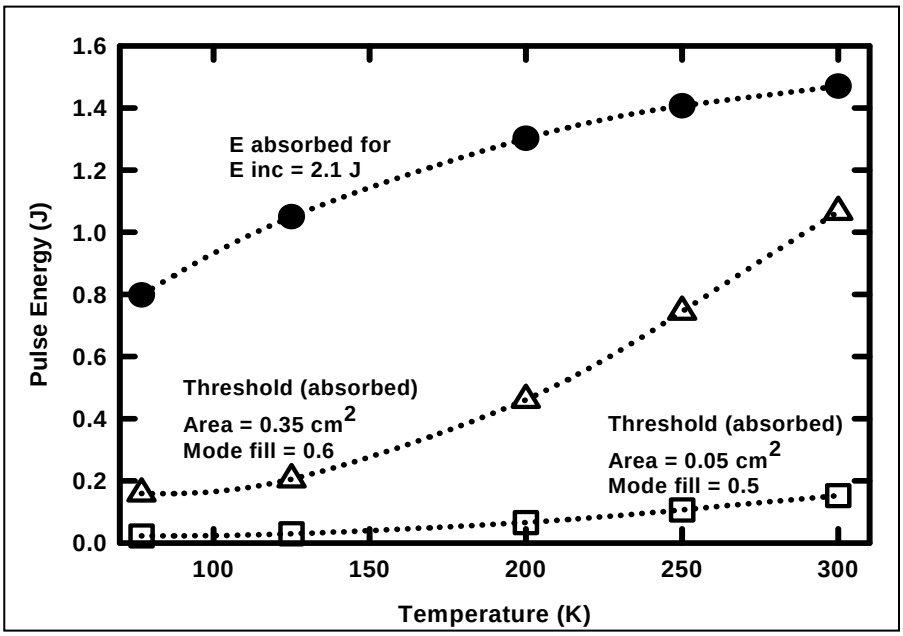

Figure 11. Er:YAG laser model results: squares and triangles: pump pulse energy absorbed at laser threshold for the two sets of parameters discussed in the text; and solid circles: pump energy absorbed for the incident pump energy used for the experimental data of figure 3.

Thus, it is likely that the optimum temperature for efficient laser action in Er:YAG is above liquid nitrogen temperature for any pump source, and more so for cases such as the present one, where the pump spectrum is broader than the absorption line. Published data on thermo-optic properties indicate that these are more favorable at 77 K than at any higher temperature (*13, 14*). Thus, a study of the trade-off between spectroscopic and thermo-optic properties would be required to find the optimum temperature for laser operation. The result will undoubtedly be

application-dependent, and will also depend on the availability and performance of spectrally narrowed laser diode pumps to better fit the absorption linewidth. We are currently investigating these trade-offs.

Although straightforward models explain the temperature dependence of the laser wavelength quite satisfactorily and of the output power (or energy) qualitatively, the pump area required to fit the energy's temperature dependence is unphysically large. Since the main effect of this large pump area is to dilute the gain, this result suggests either that the gain is substantially lower than expected or that there is some loss mechanism not accounted for in the model. We have attempted to achieve a comparable fit for a more realistic pump area by varying T in equation 2, and thus the passive loss, without success. This suggests that no temperature-independent loss mechanism is likely to explain the temperature dependence.

One possible cause for reduced gain in any laser that relies on populating the Er^{3+} $^4I_{13/2}$ manifold is upconversion. We have recently developed a model for quasi-three level laser operation that includes upconversion (*31*), and are now pursuing experiments to quantify the parameters needed to apply that model.

In summary, we have investigated the temperature dependence of resonantly diode-pumped Er:YAG laser performance from liquid nitrogen temperature to above room temperature, using a broadband (not spectrally narrowed) InGaAsP/InP diode bar stack, and the spectroscopy needed to interpret that performance. We find that the output relative to incident pump power is considerably better at low temperatures than at room temperature. Interestingly, we find that optimum output occurs at temperatures above that of liquid nitrogen, quite substantially higher with pumping by the InGaAsP/InP diode bar stack. This behavior is at least qualitatively consistent with simple laser models, but more detailed studies will be required to achieve a realistic quantitative fit to the data. Our results indicate that the optimum performance can be pushed closer to nitrogen temperature by employing diode laser pumps spectrally narrowed to be better absorbed by a single Er absorption line, as this would greatly reduce the temperature dependence of pump absorption.

7. References

1. Honea, E. C.; Beach, R. J.; Sutton, S. B.; Speth, J. A.; Mitchell, S. C.; Slkidmore, J. A.; Emanuel, M. A.; Payne, S. A. 115-W Tm:YAG Diode-Pumped Solid-State Laser. *IEEE J. Quantum Electron.* **1997**, *33*, 1592–1600.

2. Budni, P. A.; Lemons, M. L.; Mosto, J. R.; Chicklis, E. P. High-Power/High-Brightness Diode-Pumped 1.9-μm Thulium and Resonantly Pumped 2.1-μm Holmium Lasers. *IEEE J. Sel. Top. Quantum Electron.* **2000**, *6*, 629–635.

3. Fan, T. Y. Heat Generation in Nd:YAG and Yb:YAG. *IEEE J. Quantum Electron.* **1993**, *29*, 1457–1459.

4. Krupke, W. F. Ytterbium Solid-State Lasers – The First Decade. *IEEE J. Sel. Top. Quantum Electron.* **2000**, *6*, 1287–1296 and references therein.

5. Young, Y. E.; Setzler, S. D.; Snell, K. J.; Budni, P. A.; Pollak, T. M.; Chicklis, E. P. Efficient 1645-nm Er:YAG Laser. *Opt. Lett.* **2004**, *29*, 1075–1077.

6. Setzler, S. D.; Francis, M. P.; Young, Y. E.; Konves, J. R.; Chicklis, E. P. Resonantly Pumped Eyesafe Erbium Lasers. *IEEE J. Sel. Top. Quantum Electron.* **2005**, *11*, 645–657.

7. Setzler, S. D.; Francis, M. W.; Chicklis, E. P. A 100 mJ Q-switched 1645 nm Er:YAG Laser. SPIE Defense and Security Symposium, paper 6552–17, 2007.

8. Garbuzov, D.; Kudryashov, I.; Dubinskii, M. Resonantly Diode Laser Pumped 1.6-μm-Erbium-doped Yttrium Aluminum Ggarnet Solid-state Laser. *Appl. Phys. Lett.* **2005**, *86*, 131115.

9. Garbuzov, D.; Kudryashov, I.; Dubinskii, M. 110 W(0.9 J) Pulsed Power from Resonantly Diode-laser-pumped 1.6-μm Er:YAG Laser. *Appl. Phys. Lett.* **2005**, *87*, 121101.

10. Zuclich, J. A.; Gagliano, D. A.; Cheney, F.; Stuck, B. E.; Zwick, H.; Edsall, P.; Lund, D. J. Ocular Effects of Penetrating IR Laser Wavelengths. *SPIE* **1995**, *2391*, 112–125.

11. Johnson, L. F.; Geusic, J. E.; Van Uitert, L. G. Coherent Oscillations from Tm^{3+}, Ho^{3+}, Yb^{3+} and Er^{3+} Ions in Yttrium Aluminum Garnet. *Appl. Phys. Lett.* **1965**, *7*, 127–129.

12. Fork, R. L.; Walker, W. W.; Laycock, R. L.; Green, J.J.A.; Cole, S. T. Integrated Diamond Sapphire Laser. *Opt. Express* **2003**, *11*, 2532–2548.

13. Brown, D. C. The Promise of Cryogenic Solid-State Lasers. *IEEE J Sel. Top. Quantum Electron.* **2005**, *11*, 587–599.

14. Aggarwal, R. L.; Ripin, D. J.; Ochoa, J. R.; Fan, T. Y. Measurement of Thermo-optic Properties of $Y_3Al_5O_{12}$, $Lu_3Al_5O_{12}$, $YAlO_3$, $LiYF_4$, $LiLuF_4$, BaY_2F_8, $KGd(WO_4)_2$ and $KY(WO_4)_2$ Laser Crystals in the 80-300 K Temperature Range. *J. Appl. Phys.* **2005**, *98*, 103514.

15. Fan, T. Y.; Crow, T.; Hoden, B. Cooled Yb:YAG for High-power Solid State Lasers. *SPIE* **1998**, *3381*, 200–205.

16. Fan, T. Y.; Ripin, D. J.; Aggerwal, R. L.; Ochoa, J. R.; Chann, B.; Tilleman, M.; Spitzberg, J. Cryogenic Yb^{3+}-Doped Solid-State Lasers. *IEEE J. Sel. Top. Quantum Electron.* **2007**, *13***,** 448–459.

17. Dubinskii, M.; Ter-Gabrielyan, N.; Newburgh, G. A.; Merkle, L. D. Ultra-Low Photon Defect Diode-Pumped Cryo-Cooled Er:YAG Laser. *Proc. SPIE* **2007**, *6552*, 65520M.

18. Dubinskii, M.; Ter-Gabrielyan, N.; Newburgh, G. A.; Merkle, L. D. Ultra-Low-Photon-Defect Cryo-Laser Performance of Resonantly Diode-Pumped Er3+:YAG. *Conference on Lasers and Electro-Optics 2007*, paper CTuN1, 2007.

19. Ter-Gabrielyan, N.; Merkle, L. D.; Ikesue, A.; Dubinskii, M. Ultralow Quantum-defect Eye-Safe Er^{3+}:Sc_2O_3 Laser. *Opt. Lett.* **2008**, *33*, 1524–1526.

20. Shannon, R. D. Revised Effective Ionic Radii and Systematic Studies of Interatomic Distances in Halides and Chalcogenides. *Acta Cryst.* **1976**, *A32*, 751–767.

21. Gruber, J. B.; Nijjar, A. S.; Sardar, D. K.; Yow, R. M.; Russell III, C.; Allik, T. H.; Zandi, B. Spectral Analysis and Energy-level Structure of $Er^{3+}(4f^{11})$ in Polycrystalline Ceramic Garnet $Y_3Al_5O_{12}$. *J. Appl. Phys.* **2005**, *97*, 063519.

22. Sardar, D. K.; Russell III, C. C.; Gruber, J. B.; Allik, T. H. Absorption Intensities and Emission Cross Sections of Principal Intermanifold and Inter-Stark Transitions of $Er^{3+}(4f^{11})$ in Polycrystalline Ceramic Garnet $Y_3Al_5O_{12}$. *J. Appl. Phys.* **2005**, *97*, 123501.

23. Kaminskii, A. A.; Petrosyan, A. G.; Denisenko, G. A.; Butaeva, T. I.; Fedeorov, V. A.; Sarkisov, S. E. Spectroscopic Properties and 3 μm Stimulated Emission of Er^{3+} Ions in the $(Y_{1-x}Er_x)_3Al_5O_{12}$ and $(Lu_{1-x}Er_x)_3Al_5O_{12}$ Garnet Crystal Systems. *Phys. Stat. Sol. (a)* **1982**, *71*, 291–312.

24. Payne, S. A.; Chae, L. L.; Smith, L. K.; Kway, W. L.; Krupke, William F. Infrared Cross-Section Measurements for Crystals Doped with Er^{3+}, Tm^{3+}, and Ho^{3+}. *IEEE J. Quantum Electron.* **1992**, *28*, 2619–2630.

25. Koningstein, J. A.; Geusic, J. E. Energy Levels and Crystal-Field Calculations of Er^{3+} in Yttrium Aluminum Garnet. *Phys. Rev.* **1964**, *136*, A726–A728.

26. Ashurov, M. Kh.; Voronko, Yu. K., Osiko, V. V.; Sobol, A. A.; Starikov, B. P.; Timoshechkin, M. I.; Yablonskii, A. Ya. Inequivalent Luminescence Centres of Er^{3+} in Gallium Garnet Single Crystals. *Phys. Stat. Sol. (a)* **1976**, *35*, 645–649.

27. Gruber, J. B.; Quaqliano, J. R.; Reid, M. F.; Richardson, F. S.; Hills, M. E.; Seltzer, M. D.; Stevens, S. B.; Morrison, C. A.; Allik, T. H. Energy Levels and Correlation Crystal-field Effects in Er^{3+}-Doped Garnets. *Phys. Rev. B* **1993**, *48*, 15561–15573.

28. Aull, B. F.; Jenssen, H. P. Vibronic Interactions in Nd:YAG Resulting in Nonreciprocity of Absorption and Stimulated Emission Cross Sections. *IEEE J. Quantum Electron.* **1982**, *18*, 925–930.

29. Kaminskii, A. A. *Crystalline Lasers: Physical Processes and Operating Schemes*; CRC Press, Boca Raton, FL, 1996, 188.

30. Beach, R. J. CW Theory of Quasi-three Level End-Pumped LaseOoscillators. *Opt. Commun.* **1995**, *123*, 385–393.

31. White, J. O.; Dubinskii, M.; Merlke, L. D.; Kudryashov, I.; Garbuzov D. Resonant Pumping and Upconversion in 1.6 μm Er^{3+} Lasers. *JOSA B* **2007**, *24*, 2454–2460.

List of Symbols, Abbreviations, and Acronyms

CW	continuous wave
Er	erbium
F-L	Fuchtbauer-Ladenburg
GSA	ground-state absorption
InGaAs	indium gallium arsenide
InGaAsP	indium gallium arsenide phosphide
InP	indium phosphide
T	temperature
YAG	yttrium aluminum garnet
Yb	ytterbium

No of Copies	Organization
1 PDF	DEFENSE TECH INFO CTR ATTN DTIC OCA 8725 JOHN J KINGMAN RD STE 0944 FT BELVOIR VA 22060-6218
1	DARPA ATTN IXO S WELBY 3701 N FAIRFAX DR ARLINGTON VA 22203-1714
1 CD	OFC OF THE SECY OF DEFNS ATTN ODDRE (R&AT) THE PENTAGON WASHINGTON DC 20301-3080
1	US ARMY RSRCH DEV AND ENGRG CMND ARMAMENT RSRCH DEV AND ENGRG CTR ARMAMENT ENGRG AND TECHNLGY CTR ATTN AMSRD AAR AEF T J MATTS BLDG 305 ABERDEEN PROVING GROUND MD 21005-5001
1	PM TIMS, PROFILER (MMS-P) AN/TMQ-52 ATTN B GRIFFIES BUILDING 563 FT MONMOUTH NJ 07703
1	US ARMY INFO SYS ENGRG CMND ATTN AMSEL IE TD A RIVERA FT HUACHUCA AZ 85613-5300
1	COMMANDER US ARMY RDECOM ATTN AMSRD AMR W C MCCORKLE 5400 FOWLER RD REDSTONE ARSENAL AL 35898-5000
1	US GOVERNMENT PRINT OFF DEPOSITORY RECEIVING SECTION ATTN MAIL STOP IDAD J TATE 732 NORTH CAPITOL ST NW WASHINGTON DC 20402
2	UNIVERSITY OF TEXAS AT SAN ANTONIO ATTN D SARDAR ATTN J B GRUBER ONE UTSA CIRCLE SAN ANTONIO TX 78249-0697
1	US ARMY RSRCH LAB ATTN RDRL CIM G T LANDFRIED BLDG 4600 ABERDEEN PROVING GROUND MD 21005-5066
13	US ARMY RSRCH LAB ATTN IMNE ALC HR MAIL & RECORDS MGMT ATTN RDRL CIM L TECHL LIB ATTN RDRL CIM P TECHL PUB ATTN RDRL SEE O A NEWBURGH ATTN RDRL SEE O J WHITE ATTN RDRL SEE O M DUBINSKIY ATTN RDRL SEE O N TER-GABRIELYAN ATTN RDRL SEE O L MERKLE (5 COPIES) ATTN RDRL SEE O A MICHAEL ADELPHI MD 20783-1197
TOTAL 24 (22 HCs, 1 CD, 1 PDF)	

INTENTIONALLY LEFT BLANK.